Defect and Diffusion Forum
ISSN: 1662-9507, Vol. 450, pp 61-70
doi:10.4028/p-LO2XLh

Submitted: 2026-01-12
Revised: 2026-02-16
Accepted: 2026-02-22
Online: 2026-04-15

Influence of the Crystal Structure of AlCrN on Tool Coating Properties and Wear in Dry Gear Hobbing

Nils Paucke[1,a*], Martin Beutner[1,b], Andreas Lümkemann[2,c], Keith Thomas[2,d], Martin Učík[3,e], Hamid Bolvardi[2,f], Matthias Hackert-Oschätzchen[1,g]

[1]Chair of Manufacturing Technology with Focus Machining, Faculty of Mechanical Engineering, Otto von Guericke University Magdeburg, Universitätsplatz 2, 39106 Magdeburg, Germany

[2]PLATIT AG, Eichholzstrasse 9, 2545 Selzach, Switzerland

[3]PLATIT a.s., Průmyslová 3020/3, 78701 Šumperk, Czech Republic

[a*]nils.paucke@ovgu.de, [b]martin.beutner@ovgu.de, [c]a.luemkemann@platit.com, [d]k.thomas@platit.com, [e]m.ucik@platit.com, [f]h.bolvardi@platit.com, [g]matthias.hackert-oschaetzchen@ovgu.de

*corresponding author

Keywords: dry gear hobbing, wear, crystal structure, fly cutting test.

Abstract. Dry machining of gears demands advanced coating technologies to withstand high thermal and mechanical stresses. In this study, AlCrN coatings were deposited using the newly developed Focused Magnetron Sputtering (FMS) process and compared with conventional Cathodic Arc Evaporation (CAE)-AlCrN and boron-containing CAE-AlCrBN coatings. XRD analysis showed that FMS produced a fine-grained crystal structure with half the full width at half maximum (FWHM) of CAE-AlCrN. Stress-optimised deposition allowed a 60 % higher coating thickness with improved adhesion. Analogy gear hobbing tests (fly cutting tests) demonstrated that FMS-AlCrN had 52 % lower crater wear than CAE-AlCrN, while CAE-AlCrBN also improved crater-wear resistance due to boron-induced grain refinement. However, both fine-grained coatings exhibited increased flank wear compared to the coarse-grained CAE-AlCrN coating. The results show that FMS enables the production of dense, fine-grained coatings with superior adhesion and crater-wear resistance, highlighting its potential for dry gear hobbing. Further optimisation of hardness and microstructure is required to balance crater and flank wear behaviour.

Introduction

Gear hobbing is recognised as one of the most productive processes in soft machining of gears, and in recent years, there has been a clear trend towards dry gear hobbing. With the increasing demand for gears, particularly in the automotive industry, which accounts for over 41% of the gear hobbing machines [1], the trend towards dry machining becomes increasingly apparent.

Eliminating the use of cutting fluids offers economic and environmental benefits. From an economic perspective, coolant-related costs typically range from 2-8 % of total machining costs and can sometimes even surpass the costs of the tool [2]. Therefore, eliminating the need for cutting fluids offers significant potential for machining cost savings. From an environmental perspective, dry machining reduces emissions and prevents metal dust from binding with coolants [2], resulting in improved working conditions for the machine operator.

However, this transition imposes higher demands on the gear hob, mainly due to increased heat generation and challenges in chip removal, which result in faster tool wear. Consequently, advances in tool coatings are necessary. While the chemical composition, the thickness, and the architecture of coatings are traditionally considered as critical factors affecting the coating performance, recent research [3] suggests that the inherent crystalline structure of the coatings also has an impact on the coating performance. For this reason, this paper focuses on the influence of the crystal structure of AlCrN-based coatings, examining how these microstructural characteristics impact coating properties and wear during dry gear hobbing.

State of the Art

Coating technologies for gear hobs can primarily be divided into Physical Vapor Deposition (PVD) and Chemical Vapor Deposition (CVD) processes. However, PVD processes have largely superseded CVD technology for coating gear tools [4] due to several advantages, including more variety in terms of coating composition, as well as reduced processing temperatures, which enable the coating of gear hobs made of PM-HSS. Consequently, PVD processes will be further discussed.

PVD technology involves transforming the target material, which is to be deposited, into atomic particles in a vacuum environment or gaseous plasma under low-pressure conditions. These particles are then directed towards the substrate, the cutting tool to be coated, where they condense to form a coating with desired properties [5, 6]. The two most common methods for applying PVD coatings are evaporation and sputtering deposition, with Cathodic Arc Evaporation (CAE) being the leading deposition technology within the machining sector [7].

CAE operates by vaporising and ionising the target material in a high vacuum utilising an electric arc. The arc moves across the evaporator source connected as a cathode [8]. The CAE process is characteristic of a high ionisation degree of the evaporated material and a fast growth of the highly dense coatings. However, there is a main drawback of this coating technology. The CAE process tends to produce unwanted metallic droplets that can reduce the coating's density, increase the surface roughness, and act as stress concentrators, potentially leading to cracks [7, 9].

These limitations could be overcome utilising the sputtering process. In this process, an inert gas like argon is ionised under a high voltage in low-pressure plasma, allowing the charged gas ions to collide with the target material and knock off atoms through impulse exchange [8]. When utilising a magnetron, the magnetic field lines penetrate the target perpendicularly. Here, the superposition of magnetic and electric field lines causes the electrons to be deflected onto elongated spiral paths in the plasma, which lead to enhance ionisation probability and deposition rate [5,8]. A further developed process of magnetron sputtering with direct current (DCMS) is the High Power Impulse Magnetron Sputtering (HiPIMS) process. In the HiPIMS process a high power is applied in unipolar pulses, which results in a high plasma density and improved ionisation fraction, allowing for better control over the film growth [10].

Although the sputtering process and its current developments like HiPIMS have advantages over CAE in terms of droplet formation, they present a number of challenges, particularly in relation to achieving sufficient plasma densities to produce high-quality coatings on a large substrate area at an industrially practicable growth rate [7]. To overcome these challenges, PLATIT has developed a novel coating deposition technology known as Focused Magnetron Sputtering (FMS). This process is characterised by a longitudinal movement of a reduced size magnetron inside a turbular target, as shown in Fig. 1 a-b. FMS enables a sixfold increase of peak sputter power densities compared to conventional magnetron sputtering, as illustrated in Fig. 1 c. The power densities reached in the FMS process are characteristic of HiPIMS, yet with higher duty cycles, due to effective cooling in the tubular targets. This allows higher deposition rates and greater productivity. [9, 11, 12].

Recent research by Klimashin et al. [9] explored superstoichiometric $(Al,Cr)N_x$ coatings, revealing that small changes in stoichiometry significantly impact the microstructure and mechanical properties. Specifically, $(Al,Cr)N_{1.08}$ exhibited densely packed, elongated grains with a (111) growth orientation, leading to increased hardness and abrasion resistance. In contrast, $(Al,Cr)N_{1.11}$ displayed a finer-grained structure with a (220) orientation, enhancing fracture toughness and resistance to microcracking, which is beneficial for impact-intensive applications like gear hobbing.

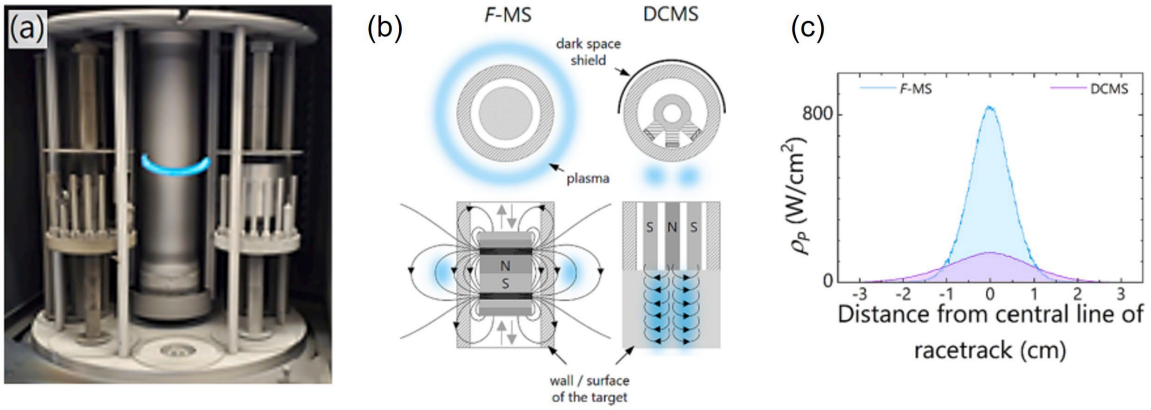

Fig. 1. (a) Platit π411 chamber with schematised annular blue plasma generated by movable focussed magnetic field, (b) Schematics of magnetron assembly for FMS and DCMS mode and (c) Power densities achieved in FMS and DCMS mode at 25 kW according to [9].

Building on these insights, this paper aims to utilise the newly developed FMS technology to influence the crystal structure of AlCrN coatings. Based on that, this study will analyse how the changes in crystal structure affect coating properties and wear resistance during gear hobbing.

Methodology

The methods for determining the coating properties involve a series of standardised tests to evaluate chemical composition, thickness, hardness, and adhesion of the coatings. The chemical composition of the coatings was determined by applying Energy Dispersive X-ray Spectroscopy (EDX). This technique involves exciting the atoms in the coating with an electron beam of specific energy, which results in the emission of X-rays characteristic of the elements present. These characteristic X-rays provide detailed information about the elemental composition of the coatings [13].

The coating thickness is assessed utilising the Calotte Grinding Test in accordance with DIN EN ISO 26423 [14]. In this test, a steel ball moistened with an abrasive fluid is utilised to grind a calotte into the coating. The grinding process forms two concentric rings on the coating surface. To calculate the coating thickness, the diagonals of these rings are measured. The ground divots were prepared using a 30 mm diameter steel ball, a 0.25 µm diameter diamond suspension and a BAQ kaloMAX grinding unit. Micrographs of the ground divots were collected utilising a Carl Zeiss Axio Scope Vario optical microscope. Measurement of divot dimensions and calculation of coating thickness was performed using Platit PQCS software.

Coating adhesion was evaluated by applying visual inspection of Rockwell Hardness test indent according to the widely used DIN 4856 norm in which HF1 represents excellent adhesion and HF6 represents total delamination of the coating [15]. A Rockwell indenter manufactured by ESI Prüftechnik GmbH was applied to perform the indentation experiments. The inspection of the indents was performed utilising the same optical microscope used for the thickness measurements. The mechanical properties of the coatings themselves were assessed by applying a Fischerscope HM2000 nanoindenter.

The crystal structure of the coating was influenced by the newly developed FMS technology. Evaluation of crystal structure was performed by sawing through approximately 90 % of the tungsten carbide substrate from the uncoated side and striking the sample with a hammer to generate a fracture surface through the remaining substrate and the coating. This fracture surface was inspected utilising a Zeiss EVO 15 Scanning Electron Microscope (SEM) to gain an impression of the coating microstructure. This microscope was equipped with an EDS detector (Xplore 30) from Oxford Instruments to evaluate the elemental composition of each coating. Furthermore, X-ray Diffraction (XRD) analysis was conducted to investigate the crystalline structure.

Alongside analysing the coating properties and crystal structure, the wear of the FMS-AlCrN coating was compared to CAE-AlCrN and CAE-AlCrBN coatings utilising the fly cutting test. The inclusion of the CAE-AlCrBN coating was motivated by the literature suggesting that boron addition can effectively reduce grain size [16,17,18]. The applied fly cutting test is an analogy test of the real gear hobbing process. Here, the gear hobbing process is characterised by a high number of cutting edges, which results in a high tool life [19]. The high productivity and tool life of gear hobs are advantageous for industry due to its cost-effectiveness but disadvantageous for basic research, as several 100 to 1,000 workpieces have to be manufactured before significant wear occurs [20]. Based on this, the fly cutting test was developed as an analogy test for research purposes. In this well-established test, the tool is reduced to a single tooth, thereby reducing the time and cost of the investigation compared to tests with a full gear hob [19]. The fly cutting tooth assumes all generating positions of the full gear hob one after the other. Based on this, the mechanical cutting load of a shifted full gear hob is correctly reproduced, and the manufactured gear is geometrically identical to the real process [20]. The experimental setup utilised for the fly cutting test is shown in Fig. 2.

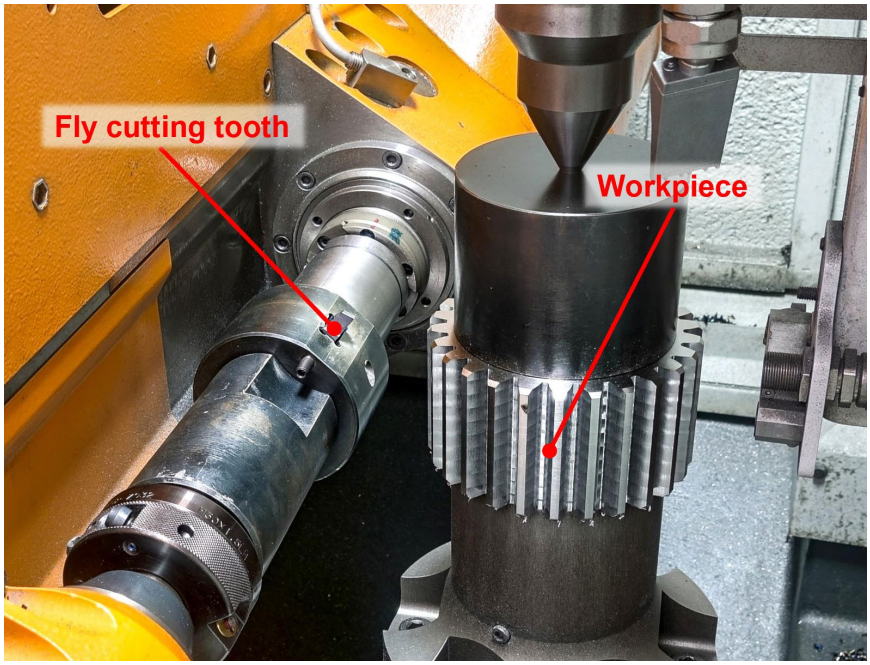

Fig. 2. Experimental setup: Fly cutting test on Liebherr LC180 gear hobbing machine.

The tests were conducted on a Liebherr LC180 gear hobbing machine. The tool substrate was made of PM-HSS (S390), and the workpiece material was made of 20MnCr5 (1.7168). The tests were conducted at a cutting speed of v_c = 220 m/min and a feed rate of f_a = 6.4 mm/rev ($h_{cu,max,Hoff}$ = 0.24 mm). The flank and crater wear were measured with an optical microscope from Mitutoyo and with an optical coordinate measuring machine µCMM from Alicona. The tests were stopped when a maximum width of the flank wear land of 130 µm or a maximum crater wear of 90 µm was reached. In this study each coating performance test was conducted once, as initial tests that were performed multiple times have shown consistent and reproducible results.

Results

All coatings were deposited utilising composite targets with a fixed Al:Cr ratio. The targets used for the FMS and CAE coatings were nominally identical, with EDX results consistently resulting in stoichiometric AlCrN with an Al:Cr ratio of around 1.6:1. For coatings containing boron, 10 at. % boron was incorporated into the target. Through appropriate selection of deposition parameters, the boron content of the coating between 2 and 4 at. % could be achieved. Precise quantification of the boron content applying EDX was not possible.

Table 1 summarises the measured coating properties, including thickness, hardness and adhesion for the investigated coatings. Due to the higher plasma density and energy input characteristic of the FMS process, a significantly thicker coating could be deposited compared to the conventional CAE process. In the present case, the FMS coating exhibits approximately 60 % greater coating thickness than the CAE-AlCrN coating. Despite the increased thickness, the FMS coating demonstrates a better adhesion class (HF2) compared to the CAE-AlCrN coating (HF3). This improvement indicates that the higher energy densities of the FMS process enable stress-optimised deposition, i.e., lower intrinsic stresses within the coating. Consequently, thicker coatings can be produced without deterioration of adhesion.

Table 1. Overview of coating properties for FMS-AlCrN, CAE-AlCrN and CAE-AlCrBN coatings.

Coating properties	Unit	FMS-AlCrN	CAE-AlCrN	CAE-AlCrBN
Coating thickness	µm	5.98	3.78	4.03
Hardness	GPa	35.7	36.9	33.9
Adhesion class	-	HF 2	HF 3	HF 2

Comparing the XRD spectra for FMS-AlCrN and CAE-AlCrN in Fig. 3, shows that the predominant texture for the FMS-AlCrN is (200), as compared to the (111) texture observed in CAE-AlCrN. XRD analysis revealed that the full width at half maximum (FWHM) of the diffraction peaks for FMS-AlCrN is also broader, suggesting a finer crystallite size. This observation is confirmed in the cross-sectional images of the coatings.

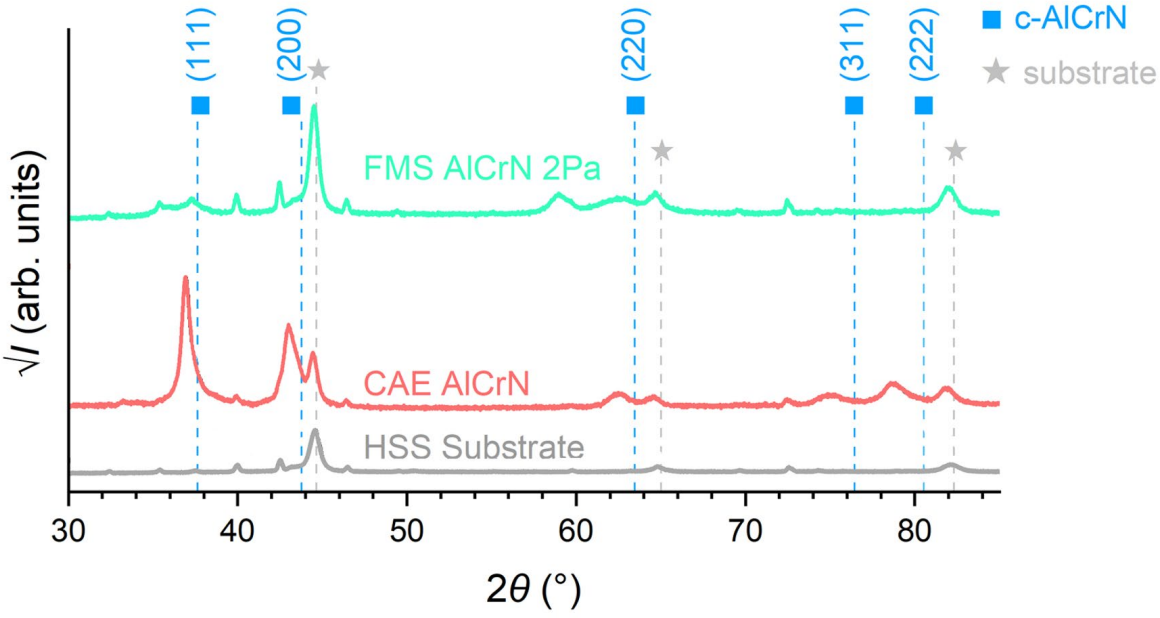

Fig. 3. X-ray diffractograms (Bragg-Brentano geometry).

Fig. 4 shows the fracture surface of the coatings after cleaving. The FMS-AlCrN coating exhibits a much finer crystalline structure while the CAE-AlCrN has a larger grain size and columnar growth pattern. As expected, the CAE-AlCrN also contains a significant number of macroparcticles and other growth defects typically associated with arc evaporation, while the FMS-AlCrN has fewer growth defects.

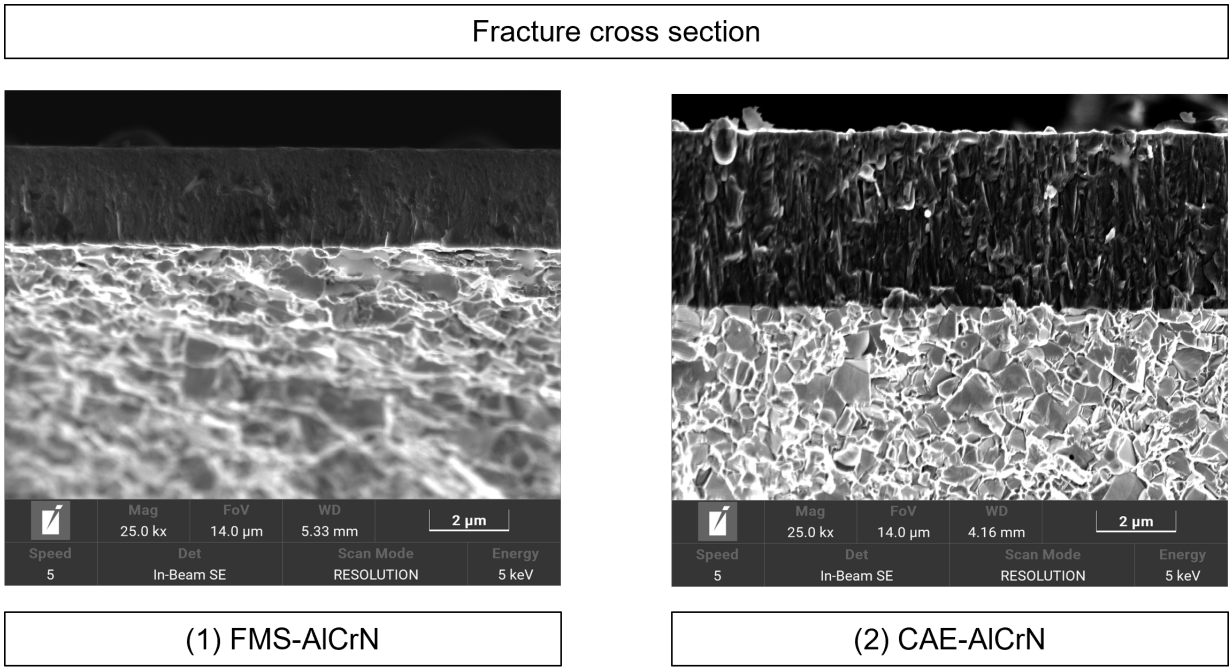

Fig. 4. Fracture cross section for (1) FMS-AlCrN and (2) CAE-AlCrN.

The macroparticles are especially obvious in the plan-view micrographs seen in Fig. 5. Interestingly, the surface topology of the FMS-AlCrN reflects the underlying fine-grained microstructure with a number of small crystalline facets visible.

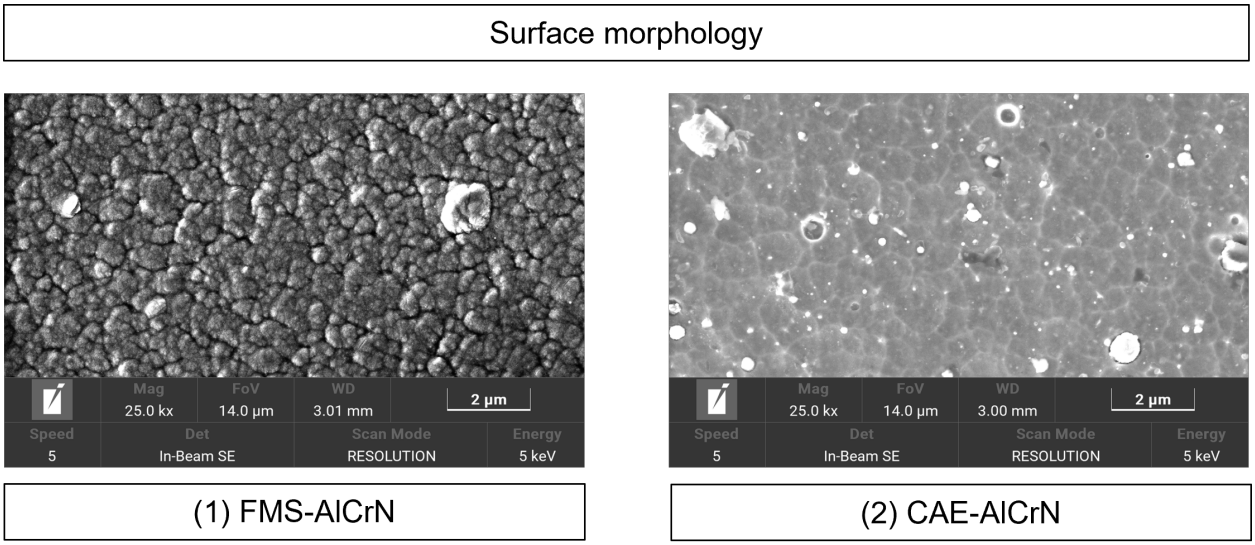

Fig. 5. Surface morphology for (1) FMS-AlCrN and (2) CAE-AlCrN.

Fig. 6 illustrates the crater wear on the rake face for the FMS-AlCrN, CAE-AlCrN, and CAE-AlCrBN coatings after constant cutting lengths of 3.1 m/tooth and 9.4 m/tooth. After a cutting length of 3.1 m/tooth, the measured crater wear depths are 8 µm for FMS-AlCrN, 14 µm for CAE-AlCrN and 11 µm for CAE-AlCrBN. For all three coatings, the wear is located close to the cutting edge, precisely at the transition between the leading flank and the tip. At this stage, the wear patterns are therefore comparable in shape and extent.

After a cutting length of 9.4 m/tooth, the differences between the coatings become evident. The crater wear increases to 50 µm for FMS-AlCrN, 104 µm for CAE-AlCrN and 28 µm for CAE-AlCrBN. For the CAE-AlCrN coating, the wear criterion is exceeded. The maximum crater wear is located on the leading flank, the region where wear initiation was first observed. On the opposite side of the rake face, at the transition from the trailing flank to the tip, a secondary crater has formed with

a maximum depth of 53 µm, which is roughly half the depth of the primary wear zone. The formation and merging of both craters were already detected after 4.7 m/tooth.

In contrast, the FMS-AlCrN coating shows significantly improved wear resistance. The maximum crater depth after 9.4 m/tooth is 50 µm, corresponding to a 52 % reduction compared to the CAE-AlCrN coating. The wear region remains similar in shape and location to that after 3.1 m/tooth, and no second crater area has formed.

The CAE-AlCrBN coating containing boron exhibits a maximum crater depth of 28 µm after 9.4 m/tooth, demonstrating a marked improvement over CAE-AlCrN. A second wear zone develops on the opposite side of the rake face. However, the two craters do not merge. The second crater appears after a cutting length of 7.8 m/tooth and shows a depth of 24 µm, slightly lower than that of the primary wear area.

Overall, both the finer microstructure of the FMS-AlCrN coating and the addition of boron in the CAE technology result in a significant reduction of crater wear. The reduced crater formation and absence or delayed development of secondary wear regions indicate improved crater wear resistance for a finer grained microstructure under dry gear hobbing conditions.

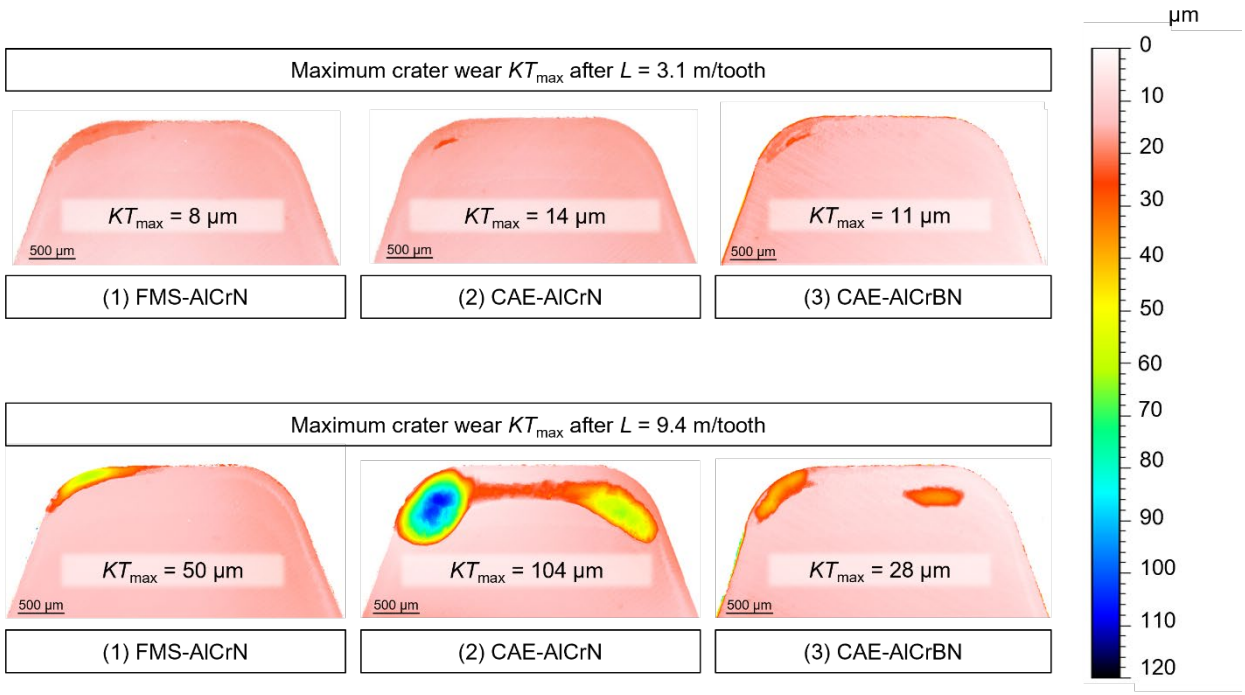

Fig. 6. Crater wear for FMS AlCrN, CAE-AlCrN and CAE-AlCrBN at a cutting length of 3.1 m/tooth and 9.4 m/tooth.

Fig. 7 shows the evolution of the maximum flank wear land (*VB*) on the leading flank as a function of the cutting length. The initial wear is the lowest for the CAE-AlCrBN coating with 16 µm, followed by CAE-AlCrN with 28 µm and FMS-AlCrN with 38 µm. Between cutting lengths of 4.7 m/tooth and 7.8 m/tooth, the increase of the maximum *VB* of both arc-deposited coatings is comparable, whereas the FMS-AlCrN coating consistently exhibits values that are approximately 25 µm higher. From a cutting length of 7.8 m/tooth onwards, the wear on the leading flank rises more rapidly for the CAE-AlCrBN coating than for the CAE-AlCrN coating, resulting in nearly identical *VB* for CAE-AlCrBN (114 µm) and FMS-AlCrN (110 µm) after 9.4 m/tooth. At a cutting length of 10.9 m/tooth, the *VB* of FMS-AlCrN reaches 146 µm, thus exceeding the wear criterion. At the same cutting length, the CAE-AlCrBN coating shows a smaller *VB* of 119 µm. Notably, the maximum wear for CAE-AlCrBN occurs further away from the tip compared to the FMS-AlCrN coating. In contrast, the CAE-AlCrN coating exhibits a maximum *VB* of 81 µm, with the wear zone located close to the tip, which corresponds to the position of the crater wear observed previously.

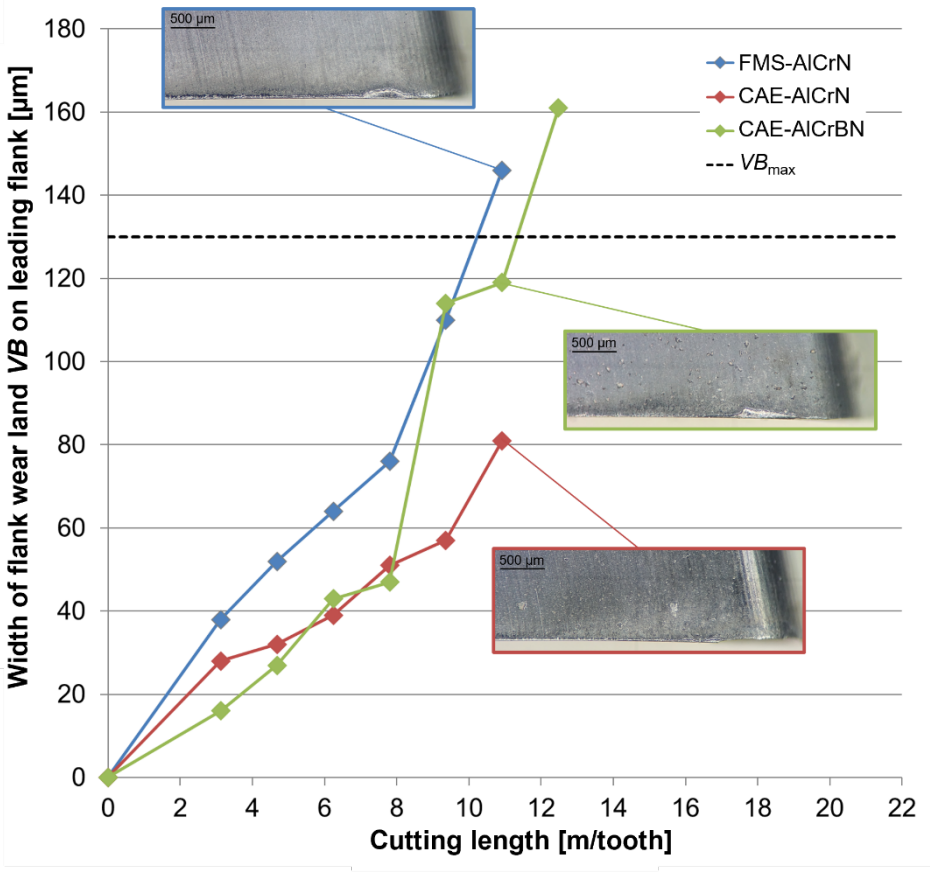

Fig. 7. Width of the flank wear land on leading flank for FMS-AlCrN, CAE-AlCrN and CAE-AlCrBN coating.

Based on the wear analysis on the leading flank, grain refinement achieved either through FMS technology or through the addition of boron has a potentially negative influence on flank-wear resistance. For both FMS-AlCrN and CAE-AlCrBN coatings, the wear criterion was reached primarily due to abrasive flank wear. Conversely, the coarser-grained CAE-AlCrN coating demonstrated lower flank wear and remained clearly below the critical wear threshold VB_{max} at the end of the cutting test.

Discussion and Outlook

With the newly developed Focused Magnetron Sputtering technology, it was possible to produce an AlCrN coating with a fine-grained crystal structure. XRD analysis revealed that the FWHM of the FMS-AlCrN coating was only about half of that of the conventional CAE-AlCrN coating, indicating a significant grain refinement. In addition, stress-optimised deposition by FMS enabled a considerably higher coating thickness while simultaneously improving adhesion compared to the CAE-AlCrN coating. Contrary to expectations, the finer microstructure did not result in an increase in coating hardness. To further investigate the influence of grain refinement, an additional CAE-AlCrBN coating was examined during the fly cutting tests, as literature reports suggest that the addition of boron can promote finer grains.

The wear experiments demonstrated that a finer crystalline structure improves crater-wear resistance. This effect can be explained by the longer crack propagation paths in fine-grained microstructures, which delay crack growth and material removal. In contrast, the coarse-grained CAE-AlCrN coating exhibited higher abrasion resistance against flank wear than both the FMS-AlCrN and the CAE-AlCrBN coatings. A possible explanation is that fine-grained structures may be more easily polished away near the cutting edge, enhancing abrasive wear. Another contributing factor could be the lower hardness measured for both FMS-AlCrN and CAE-AlCrBN coatings, which may have promoted flank wear.

In future studies, the influence of microstructure on flank wear should be systematically investigated by comparing coatings with similar hardness but different grain sizes. If the results reveal that hardness has the predominant effect, the next step should be the development of an FMS-deposited coating combining both fine-grained structure and increased hardness to simultaneously meet the requirements for abrasion resistance and crack resistance. If, however, the microstructure proves to be the dominant factor, an optimal “sweet spot” in grain size and coating architecture must be determined to balance crater and flank wear performance.

References

[1] https://www.industryresearch.biz/market-reports/gear-cutting-machines-market-102160, checked: 08.10.2025.

[2] R. Schestag, Trockenbearbeitung in der Praxis, Landesgewerbeamt Baden-Württemberg, Stuttgart, 2004.

[3] F. F. Klimashin, M. Učík, M. Matas, D. Holec, M. Beutner, M. Hackert-Oschätzchen, A. Xomalis, J. J. Schwiedrzik, J. Klusoň, M. Jílek, A. Lümkemann, J. Michler, T. E. J. Edwards, Superstoichiometric (Al,Cr)N: Nitrogen's whereabouts and role in structure-property relationships: submitted to Acta Materialia 294 (2025). https://doi.org/10.1016/j.actamat.2025.121158.

[4] W. Kalss, Latest Developments and Applications in Coating Technologies. in: First International HSS Forum Conference, Aachen, 2005.

[5] A. Baptista, F. J. G. Silva, J. Porteiro, J. L. Miguez, G. Pinto, L. Fernandes, On the Physical Vapour Deposition (PVD): Evolution of Magnetron Sputtering Process for Industrial Applications, in: 28th International Conference on Flexible Automation and Intelligent Manufacturing, 2018. https://doi.org/10.1016/j.promfg.2018.10.125.

[6] D. M. Mattox, The foundations of Vacuum Coating Technology, W. Andrew, Noyes Publications, UK, USA, 2003. ISBN: 0-8155-1495-6.

[7] J. Klusoň, M. Učík, E. Jankes, K. Thomas, H. Bolvardi, A. Lümkemann, Focused magnetron sputtering (FMS): Combining HiPIMS-level plasma density and DCMS deposition rates on large industrial targets, in: Journal of hp tooling, 2025. ISSN 2628-5444.

[8] F. Klocke, Fertigungsverfahren 1: Zerspanung mit geometrisch bestimmter Schneide, Springer Vieweg, VDI Buch, Berlin, 2018. ISBN: 978-3-662-54207-1.

[9] F. F. Klimashin, J. Klusoň, M. Učík, R. Žemlička, M. Jílek, A. Lümkemann, J. Michler, T. E. J. Edwards, High-power-density sputtering of industrial-scale targets: Case study of (Al,Cr)N: submitted to Materials & Design (237), 2024. https://doi.org/10.1016/j.matdes.2023.112553.

[10] J. T. Gudmundsson, N. Brenning, D. Lundin, U. Helmersson, High power impulse magnetron sputtering discharge, in: J. Vaxc. Sci. Technol. A30, 2012. https://doi.org/10.1116/1.3691832.

[11] J. E. Greene, Review Article: Tracing the recorded history of thin-film sputter deposition: From the 1800s to 2017, in J. Vac. Sci. Technol. A 35, 2017. https://doi.org/10.1116/1.4998940.

[12] R. De Gryse, J. Haemers, W. P. Leroy, D. Depla, Thirty years of rotatable magnetrons, in: Thin Solid Films (520), 2012. https://doi.org/10.1016/j.tsf.2012.04.065.

[13] H. Biermann, L. Krüger, Moderne Methoden der Werkstoffprüfung, John Wiley & Sons, 2014. ISBN 978-3-527-67070-3.

[14] DIN EN ISO 26423: 2016-11: Hochleistungskeramik – Bestimmung der Schichtdicke mit dem Kalottenschleifverfahren (ISO 26423:2009); Deutsche Fassung EN ISO 26423:2016. https://dx.doi.org/10.31030/2482914.

[15] DIN 4856: 2018-02: Kohlenstoffschichten und andere Hartstoffschichten – Rockwell-Eindringprüfung zur Bewertung der Haftung. https://dx.doi.org/10.31030/2795562.

[16] T. Sato, T. Yamamoto, H. Hasegawa, T. Suzuki, Effects of boron contents on microstructures and microhardness in CrxAlyN films synthesized by cathodic arc method, in: Surface & Coatings Technology (201), 1348-1351, 2006. https://doi.org/10.1016/j.surfcoat.2006.01.068.

[17] C. Tritremmel, R. Daniel, M. Lechthaler, H. Rudigier, P. Polcik, C. Mitterer, Microstructure and mechanical properties of nanocrystalline Al–Cr–B–N thin films, in: Surface & Coatings Technology (213), 1-7, 2012. https://doi.org/10.1016/j.surfcoat.2012.09.055.

[18] A. Lümkemann, M. Jílek, T. Cselle, D. Blösch, Stress optimized hard coatings for high-perfomance gear hobbing, Seminar: Trends in Gear Soft Manufacturing, Aachen, 2018.

[19] F. Klocke, C. Brecher, Zahnrad- und Getriebetechnik: Auslegung – Herstellung Untersuchung – Simulation, München, Carl Hanser Verlag, 2017. https://www.hanser-elibrary.com/doi/book/10.3139/9783446431409.

[20] M. Beutner, Ein Beitrag zum Temperaturverhalten und zur thermischen Belastung beim trockenen Wälzfräsen, Magdeburg, Univ., Diss., 2019. http://dx.doi.org/10.25673/14020.